Chapter 5

Optimal Size and Placement of Actuators and Sensors

5.1 Introduction

One of the limitations of a piezoelectric material is the amount of force it can exert. Hence, it is important to optimize the locations and sizes of the actuators so that the required control effort is minimum. Similarly, to obtain a good signal to noise ratio, sensors should be chosen to provide maximum output for the vibration in the modes of interest. These problems become more critical as the number of actuators and sensors increases and the mode shapes become more complicated. We saw in Chapter 4 that an inflated torus has several modes having close (or exactly the same) frequencies. This makes it necessary to use multiple actuators and sensor. Unlike the case of a beam or plate, the mode shapes were also found to be quite complicated. For the same reasons, we will see that the modal interactions of actuators and sensors are also quite complicated. Therefore, we will use optimization techniques to find a good set of actuators and sensors. Out of several optimization

techniques, we choose a genetic algorithm (GA), as it can produce a global optimum solution and can be applied to complicated problems with relative ease.

In Chapter 3, we derived analytical expressions for the modal forces and modal sensing constants using the actuator and sensor equations along with the equations of motion. In this chapter, we numerically evaluate these expressions to find the modal forces and modal sensing constants for a particular actuator and sensor. These quantities give information regarding the individual modes. In order to obtain a cumulative performance measure of all the considered modes, controllability and observability indices are defined. These indices will be called performance indices. Thereafter, a parametric study is conducted in order to understand the effects of locations and sizes of the actuator and sensor on the modal forces, modal sensing constants, and performance indices. These studies show behaviors of actuators and sensors in the modal domain and also give clues for finding optimal actuators and sensors. It also suggests that it would be difficult to find a closed-form solution for the optimal locations and sizes of several actuators and sensors considering more than a few modes. For this reason, we will be using a genetic algorithm. This method is explained briefly and then applied for the case of one actuator and one sensor so as to demonstrate the advantage of optimal actuator and sensor. After that, the algorithm is applied for finding five actuators and five sensors. These optimal actuators and sensors will be used in Chapter 6 where the vibration control problem is attempted. Up to this point, we have not considered the effects of stiffness and mass of the piezoelectric patches, called passive effect. In reality, one needs to consider the passive effects of the actuators and sensors. We calculate the natural frequencies and mode shapes of the inflated torus attached with the piezoelectric patches. In the control problem, we will be using these changed natural frequencies and mode shapes in order to have a more accurate system model.

5.2 Modal Forces and Modal Sensing Constants

Compared to PVDF material, MFC^{TM} has much higher stiffness and density (Tables 5.1 and 5.2). This makes the passive effects of MFC^{TM} higher than those of PVDF and making it capable of changing the dynamic characteristics of the inflated torus, as we will see later in this chapter. In this study, MFC^{TM} patches will be used as actuators and PVDF patches will be used as sensors. The actuator's *1*-direction is assumed to be aligned with the *s*-direction of the torus. In Chapter 3, we presented derivations for unimorph and bimorph actuators. It should be noted that due to the closed nature of the complete torus, it is quite difficult to fabricate a bimorph-type of actuator. Apart from this, we also found that, due to very small wall-thickness of the torus, the induced stress couples (bending moments) are very small (10^{-5} times less) compared to induced in-plane stress resultants. Also, for the same number of actuators, the in-plane stress resultants are almost the same in both unimorph and bimorph configurations. Hence, we will work with unimorph actuators.

Table 5.1: Data for MFC^{TM} actuator.

Parameter	**Values**
Elastic modulus (E_1^p), N/m^2	$3.45\mu 10^{10}$
Elastic modulus (E_2^p), N/m^2	$7.58\mu 10^{9}$
Shear modulus (G_{12}^p), N/m^2	$1.46\mu 10^{10}$
Wall-thickness (h_p), m	$23.37\mu 10^{-5}$
Poisson's ratio (ν_{12}^p)	0.25
Density (ρ_p), Kg/m^3	7552
Piezoelectric strain constant (d_{11}), m/V	$53\mu 10^{-11}$
Piezoelectric strain constant (d_{12}), m/V	$-21\mu 10^{-11}$
Spacing between the interdigitated electrode (t_p), m	0.001

Table 5.2: Data for the PVDF sensor.

Parameter	Values
Elastic modulus (E_1^p , E_2^p), N/m^2	$2.0\mu 10^9$
Wall-thickness (h_p), m	$28\mu 10^{-6}$
Poisson's ratio (ν_{12}^p)	0.29
Density (ρ_p), Kg/m^3	1800
Piezoelectric constant (h_{31} , h_{32}),V/m	$4.32\mu 10^8$

Now, we present numerical values of the modal forces for an arbitrarily chosen size and location of an MFC^{TM} actuator. Figure 5.1-a shows the actuator location on the torus and Fig. 5.1-b is the bar chart showing the absolute values of modal forces for unit actuator voltage. A noticeable point is that the actuator does not show the same authority on all modes. While the modal forces corresponding to modes 5, 7, and 9 can be seen to be high, the modal forces for other modes are relatively smaller. It is also quite possible that the modal forces for some modes are zero for a particular actuator, leading to no control authority of the actuator on those modes. The modal characteristics play an important role in determining the modal forces. We discuss this point in detail in the next section.

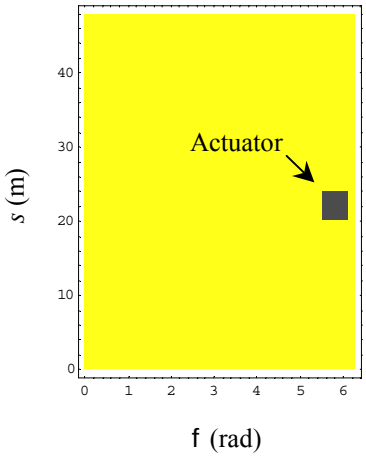

(a) Location and size of an actuator.

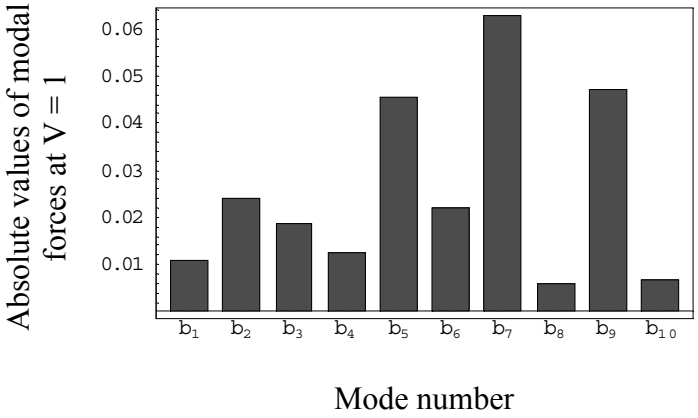

(b) Modal controllability of the actuator.

Fig. 5.1: Modal forces due to an MFC^{TM} actuator.

Figure 5.2 presents the modal sensing constants for an arbitrary sensor. While the sensing for modes 4 and 7 are quite big, the constants for modes 2, 6, and 3 are relatively small. Similar to the modal forces, it should be noted here that a higher sensing constant gives higher modal observability and vice versa.

Basically, Figs. 5.1-b and 5.2-b present the elements of the input matrix (B) and the output matrix (C), respectively. Zero elements of these matrices could make the system uncontrollable and unobservable, making the controller and observer ineffective.

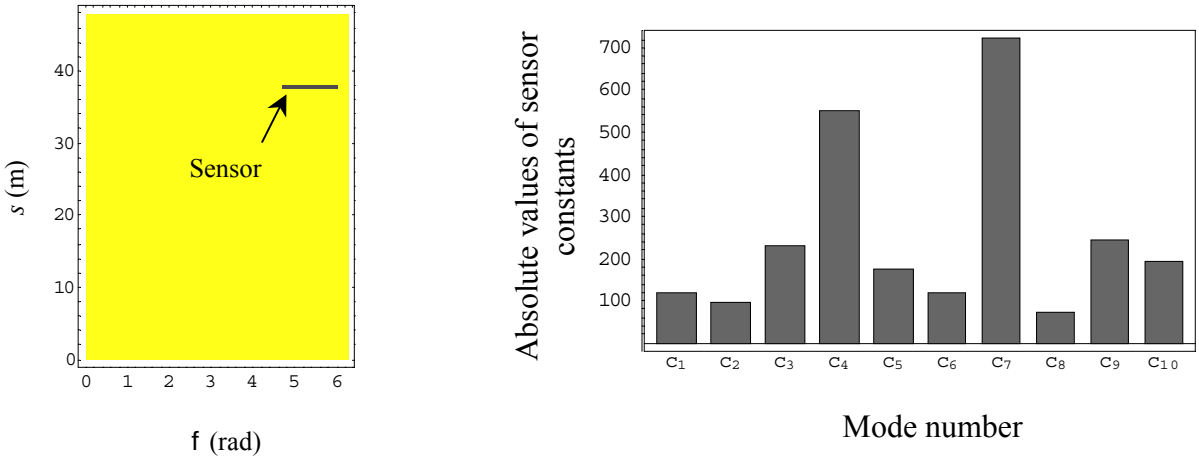

(a) Location and size of a sensor.

(b) Modal observability of the sensor.

Fig. 5.2: Modal sensing constants of a PVDF sensor

5.3 Performance Indices

The modal forces and the modal sensing constants give information regarding the interaction of individual modes with the actuators and sensors. However, a cumulative performance measure is needed that can predict the overall performance of the actuators and sensors. From linear control theory, it can be seen that the controllability (observability) of a linear system can be determined by calculating the controllability (observability) grammian.

If it is nonsingular, the system is said to be controllable (observable) with that set of actuators (sensors). Since this concept is of binary nature, it cannot be effectively applied in evaluating the performance of distributed actuators and sensors. For example, if a system is non-controllable (non-observable) for a particular actuator (sensor) location, it can be made controllable (observable) by shifting the location by a small amount. However, in this case, the control effort exerted by the actuator will be huge for an effective control (similarly, the sensor voltage will be very small, although nonzero). In this section, we describe performance indices, which are based upon the eigenvalues of controllability and observability grammian matrices that minimizes the control energy requirement and maximizes the energy of sensor signals (Hac, and Lui, 1993). These indices will be used later in finding optimal actuators and sensors. The state-space model, as given by Eqs. (3.41), is

$$\dot{\boldsymbol{x}} = \boldsymbol{A}\,\boldsymbol{x} + \boldsymbol{B}\,\boldsymbol{u}\,, \qquad\qquad \boldsymbol{y} = \boldsymbol{C}\,\boldsymbol{x}\,, \tag{5.1}$$

where $\boldsymbol{u}$ is the actuator voltage and $\boldsymbol{y}$ is the sensor voltage. The matrices $\boldsymbol{A}$, $\boldsymbol{B}$, and $\boldsymbol{C}$ can be derived appropriately from Eqs. (3.37) and (3.39). Now, we define the problem of minimum control energy requirement to regulate the system from an initial state, $\boldsymbol{x}(0)$, to a final state, $\boldsymbol{x}(t_f)$ as (Hac, and Lui, 1993)

$$\text{Minimize} \qquad J_c = \int_0^{t_f} \boldsymbol{u}^T(t)\,\boldsymbol{u}(t)dt\,. \tag{5.2}$$

Using Pontryagin's minimum principle (Meirovitch, 1990) the solution of Eq. (5.2) is

$$(J_c)_{\min} = [e^{\boldsymbol{A}t_f}\,\boldsymbol{x}(0) - \boldsymbol{x}(t_f)]^T\,\boldsymbol{W}_{\boldsymbol{c}}(t_f)^{-1}[e^{\boldsymbol{A}t_f}\,\boldsymbol{x}(0) - \boldsymbol{x}(t_f)] \tag{5.3}$$

where

$$\boldsymbol{W}_c(t_f) = \int_0^{t_f} e^{\boldsymbol{A}\tau}\,\boldsymbol{B}\,\boldsymbol{B}^T\,e^{\boldsymbol{A}^T\tau}d\tau\,, \tag{5.4}$$

The matrix $\boldsymbol{W_c}(t_f)$ is called the controllability grammian matrix and it depends upon the input matrix $\boldsymbol{B}$. Maximizing a norm of the controllability grammian matrix would lead to the minimum control energy requirement. In addition, a small eigenvalue of the controllability grammian matrix would lead to at least one mode requiring very high control effort. This implies that all the eigenvalues of the controllability grammian matrix should be as high as possible. It is also more desirable to have the condition of minimum energy requirement be independent of the final time, t_f. A grammian matrix independent of t_f is obtained using the following relation:

$$\boldsymbol{W_c}(t_f) = \boldsymbol{W_c}(\infty) - e^{\boldsymbol{A}t_f}\boldsymbol{W_c}(\infty)e^{\boldsymbol{A}^T t_f} . \tag{5.5}$$

For a stable system, as t_f increases, the effect of the second term in the above equation decreases and hence it is appropriate to impose the minimization problem based upon $\boldsymbol{W_c}(\infty)$, which is independent of the final time. The matrix $\boldsymbol{W_c}(\infty)$ can be calculated by solving the Lyapunov equation

$$\boldsymbol{A}\boldsymbol{W_c}(\infty) + \boldsymbol{W_c}(\infty)\boldsymbol{A}^T + \boldsymbol{B}\boldsymbol{B}^T = 0 . \tag{5.6}$$

The eigenvalues of the matrix $\boldsymbol{W_c}(\infty)$ play a crucial role in determining the performance of the actuator. Based upon the observations about the eigenvalues, we define the following performance index (PI_c) (Hac, and Lui, 1993; Leleu, Abou-Kandil, Bonnassieux, 2000):

$$PI_c = \frac{1}{\sigma(\lambda_i)}\left(\sum_{i=1}^{2N}\lambda_i\right)\sqrt[2N]{\prod_{i=1}^{2N}(\lambda_i)} , \tag{5.7}$$

where λ_i are the eigenvalues of $\boldsymbol{W_c}(\infty)$ and $\sigma(\lambda_i)$ is the standard deviation of λ_i. A high value of the standard deviation implies that the eigenvalues are widely separated and hence some of them are less controllable and some of them are more controllable. A case where all

the modes are almost equally controllable is preferable. This leads to a very low standard deviation and hence a high performance measure (Leleu, Abou-Kandil, Bonnassieux, 2000). The summation term in Eq. (5.7) represents the size of the grammian and should be large for good performance. To ensure that all the eigenvalues of the grammian are high (for good controllability of each mode), the performance index includes the product of all the eigenvalues.

From the duality of controllability and observability, we can derive a similar expression for the performance index (PI_o) for the sensor. The objective here would be to maximize the energy of the sensor signal:

$$\text{Maximize} \qquad J_o = \int_0^{t_f} \boldsymbol{y}^T(t)\, \boldsymbol{y}(t) dt \,. \tag{5.8}$$

This leads to the observability grammian matrix, $\boldsymbol{W_o}(\infty)$, defined as

$$\boldsymbol{W_o}(\infty) = \int_0^{\infty} e^{\boldsymbol{A}\tau} \boldsymbol{C}^T \boldsymbol{C}\, e^{\boldsymbol{A}^T\tau} d\tau \,. \tag{5.9}$$

The observability grammian is also the solution of the Lyapunov equation

$$\boldsymbol{A}^T \boldsymbol{W_o}(\infty) + \boldsymbol{W_o}(\infty)\boldsymbol{A} + \boldsymbol{C}^T \boldsymbol{C} = 0 \,. \tag{5.10}$$

An equation similar to Eq. (5.7) can be written for PI_o where λ_i would be eigenvalues of the observability grammian matrix $\boldsymbol{W_o}(\infty)$. Definitions of controllability and observability indices will be used in finding the locations and sizes of the actuators and sensors, respectively. The closed-form solutions of Lyapunov equations can be found by some matrix manipulations (Williams, 1990).

5.4 Parametric Study

We saw that the modal forces and modal sensing constants can be related to the performances of the actuators and sensors. In this section, we will study how actuator and sensor sizes and locations influence the modal forces, modal sensing constants, controllability index, and observability index. These studies will also reveal how these parameters are affected by the modal characteristics (symmetry, wave number). Unless mentioned otherwise, the coordinates ϕ_1, ϕ_2, s_1, and s_2 of the actuator and sensor will be 0, $\pi/8$, 0, and $\pi R/8$. We consider the first ten modes in this study. Since the behaviors of repeated modes will be similar, we consider only one of the two repeated modes.

First, we examine the behavior of an actuator. Location of the actuator will be defined as the location of its center. Figure 5.3-a shows the modal forces and performance index of the actuator when its position is changed around the cross-section of the torus. As expected, they are periodic. While some of the modal forces are symmetric about 0^o and 180^o, the others are antisymmetric. The reason can be explained by inspecting the constituents of the modal forces. In Chapter 4, we performed the free vibration analysis of the inflated torus and presented mode shapes as well as the corresponding frequencies, wave number, and the nature of symmetry (Fig. 4.5). From Eq. (3.38), one can see that the modal forces consist of three terms containing three displacements $U^k(\phi,s)$, $V^k(\phi,s)$, and $W^k(\phi,s)$. After substituting the expressions for equivalent actuator forces, Eqs. (3.30), one can analyze the three terms to determine the behaviors of the modal forces. It can be seen that the first term contains the difference of the slopes of $U^k(\phi,s)$ in the ϕ-direction evaluated at ϕ_2 and ϕ_1, the second term contains the difference of the slopes of $V^k(\phi,s)$ in the s-direction evaluated at s_2 and s_1, and the third term contains the integrations of the normal deflection, $W^k(\phi,s)$. The superscript k denotes the k^{th} mode. Note that the derivative of the Lamé parameter A_s will be antisymmetric and the actuator-induced bending moment resultants can be neglected compared to the actuator-induced in-plane stress resultants. Now, using the properties of symmetric and antisymmetric functions and after performing some

more simplifications, one can conclude that the symmetric and the antisymmetric modes will produce symmetric and antisymmetric modal forces. Hence, in Fig. 4.3, we see that the modal forces corresponding to modes 2, 5, 7, and 9 are symmetric and the others (1, 3, 4, 6, 8, 10) are antisymmetric. If we draw a vertical line through $\phi = 180^o$, we observe that the symmetrical modes on one side of the line are the mirror image of the other side. On the other hand, the antisymmetric modal forces assume the negative of their mirror images and hence their values at $\phi = 0^o$, 180^o, and 360^o are exactly zero.

A node in a vibration mode is defined as a location where the deflection is always zero. The location of a node can be easily computed for the case of structures like beams and plates. Forces acting upon a node cannot affect the dynamics of the beam in that mode. A similar conclusion can be drawn in the case of a torus. However, as explained earlier, the modal forces depend upon all three deflections. This implies that the concept of a node is more complicated in the case of a torus. Nonetheless, locations where the modal forces are zero will behave as the nodes of the torus. If a patch is attached at a neighborhood of this location, it will require a huge control voltage to change the dynamics in that mode. In Fig. 5.3-a we see that the antisymmetric modal forces become zero at $\phi = 0^o$, 180^o, and 360^o. Due to this, the controllability indices corresponding to $\phi = 0^o$, 180^o, and 360^o also become zero (Fig. 5.3-b). On the other hand, it shows peaks at $\phi = 75^o$, 120^o, 240^o, and 285^o, demonstrating high performance of the actuator at these locations. This is because at these locations the actuator shows good control authority on the ten modes. The symmetry in the plot of controllability index signifies the symmetric structure of the torus around the plane passing through $\phi = 0^o$ and 180^o.

Figure 5.4 shows the modal forces and the controllability index when the angular width of the actuator patch is varied from 0^o to 360^o along the tube. All the modal forces due to the antisymmetric modes increase up to 180^o and decrease thereafter. It is interesting to note that modal force 7, due to the axisymmetric symmetric mode, is always non-zero.

Also, in Fig. 5.1, this modal force is largest, making the mode easily controllable from any location around the tube. From the plot of controllability index, it clear that a patch that will cover the tube completely is no good as it will lead to zero performance index of the actuator.

Figure 5.5 demonstrates the behavior of an MFC^{TM} patch as its location is changed along the *s*-direction. The number of cycles of the modal forces in the *s*-direction depends upon the wave number of the corresponding mode. For example, the first mode has a wave number of two and hence exhibits two complete cycles in the range 0^o to 360^o. The modal forces 4 and 7 remain constant, as they are axisymmetric and hence do not depend upon *s*. Since the torus is symmetric around the axis of rotation, the behavior of an actuator should not change along the *s*-direction. This is indeed true. Due to the symmetric nature of the torus, we get two repeated frequencies corresponding to any non-axisymmetric mode. The two frequencies are related to two modes orthogonal to each other (Fig. 4.2). In Fig. 5.5, we only considered one of the orthogonal modes and hence the behaviors of the actuators are changing. Once the other mode of the pair is concerned, location of an actuator will not change its behavior as it is moved along the circumference of the torus. If there are more than one actuator, then as long as the separations between them are kept constant, it will not matter where they are put along the *s*-direction.

The effect of patch length along the *s*-direction is shown in Fig. 5.6. We see that as the actuator length increases in the *s*-direction, the modal forces due to non-axisymmetric modes behave in cyclic fashion, again due to the particular dependency of displacement function in the *s*-direction. In contrast, while the modal force 7 keeps increasing, modal force 4 decreases continuously because of its axisymmetric nature.

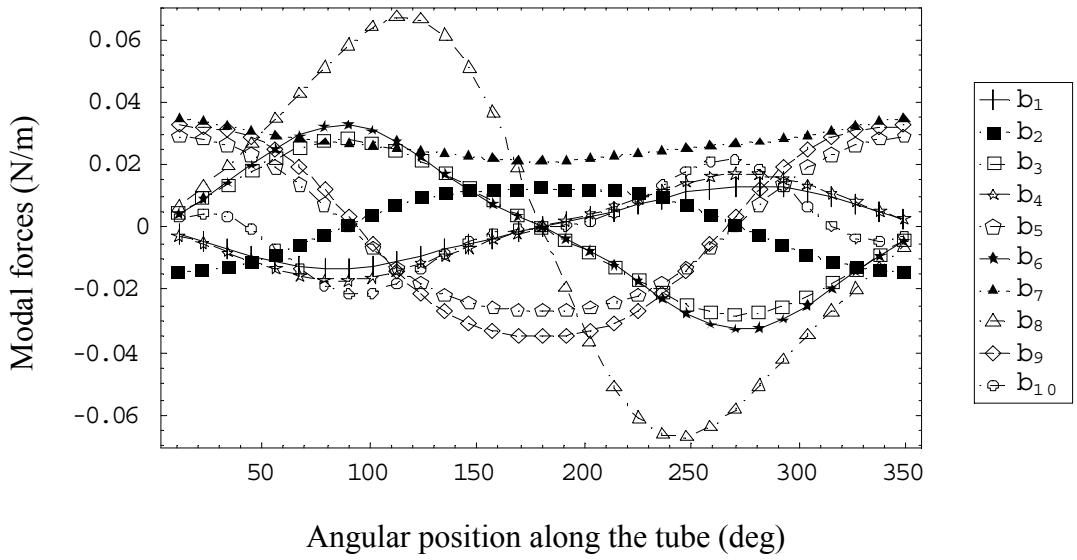

(a)

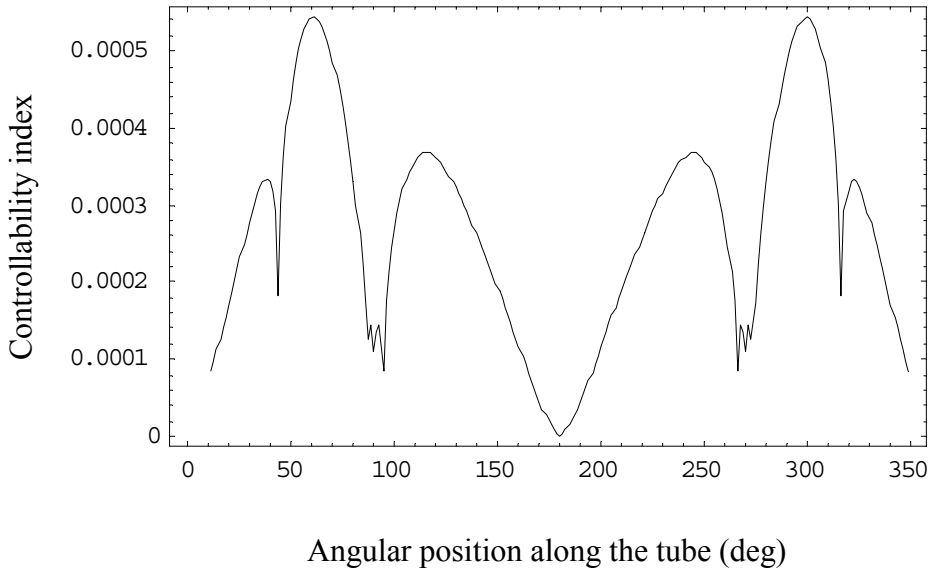

(b)

Fig. 5.3: Modal forces at unit voltage and controllability index as the location of an actuator is changed from $\phi = 0$ to 360^o along the tube of the torus.

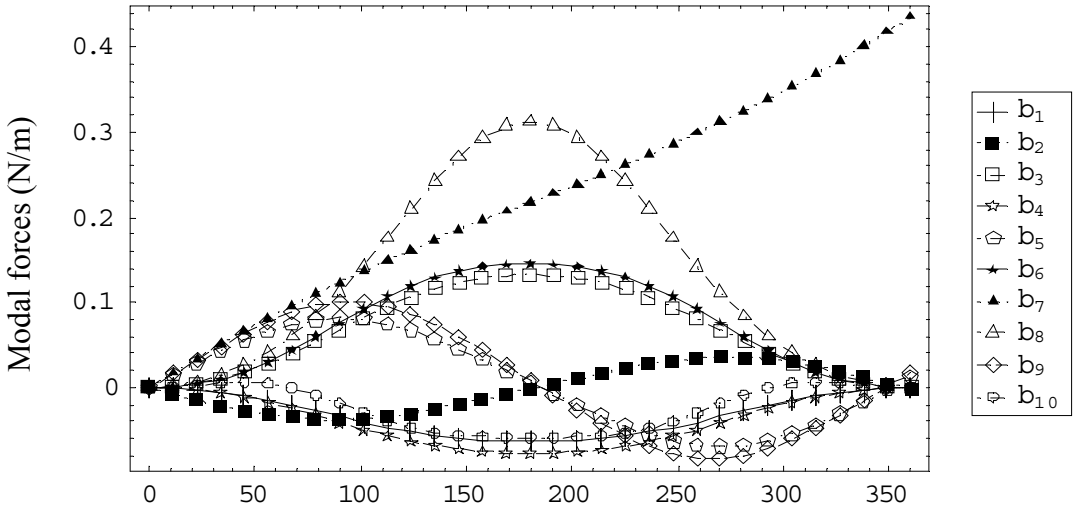

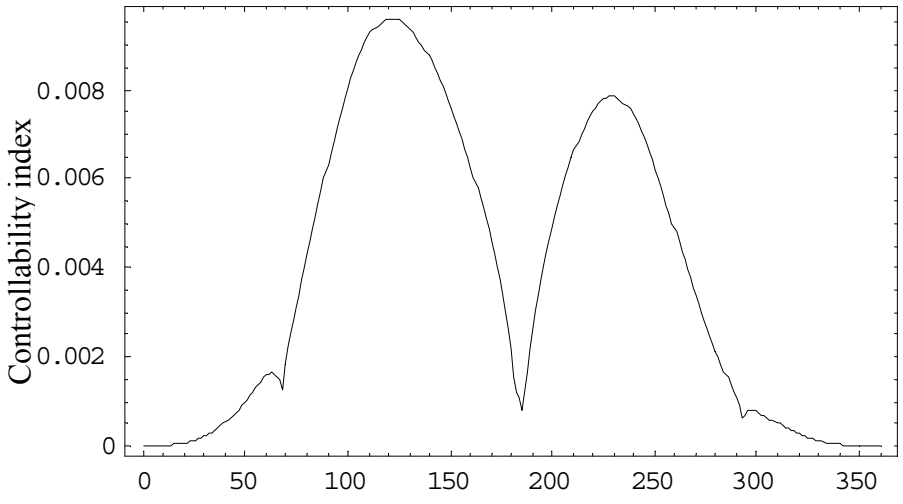

Fig. 5.4: Modal forces at unit voltage and controllability index for an actuator as its angular width f_2 varies from 0 to 360^o along the tube of the torus.

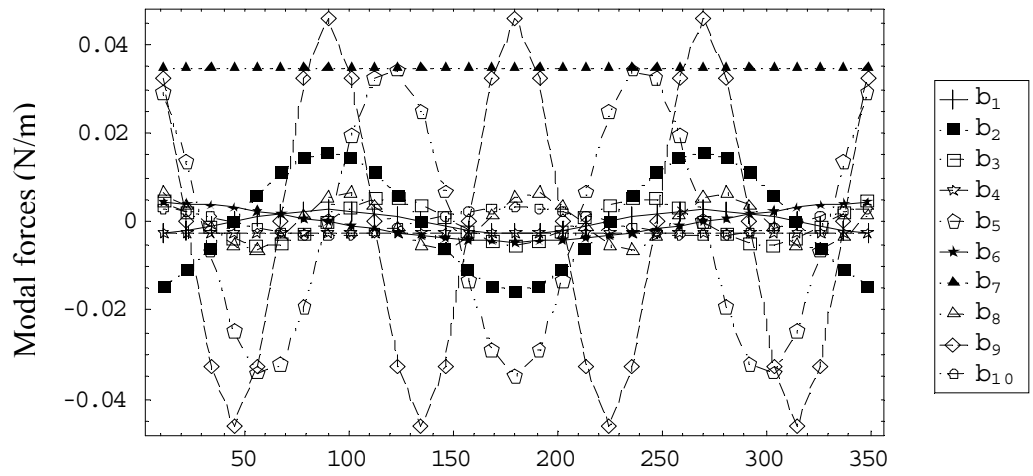

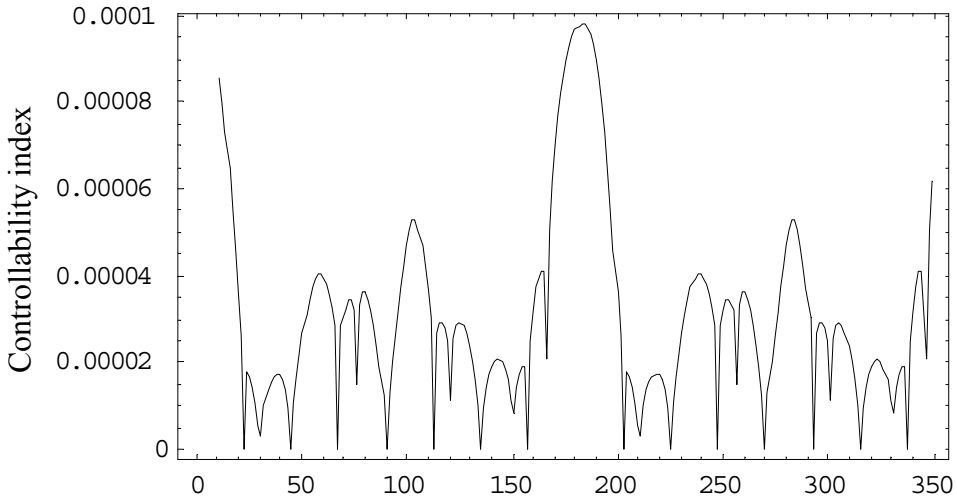

Fig. 5.5: Modal forces at unit voltage and controllability index as the location of an actuator is changed from $q = 0$ to 360^o along the torus.

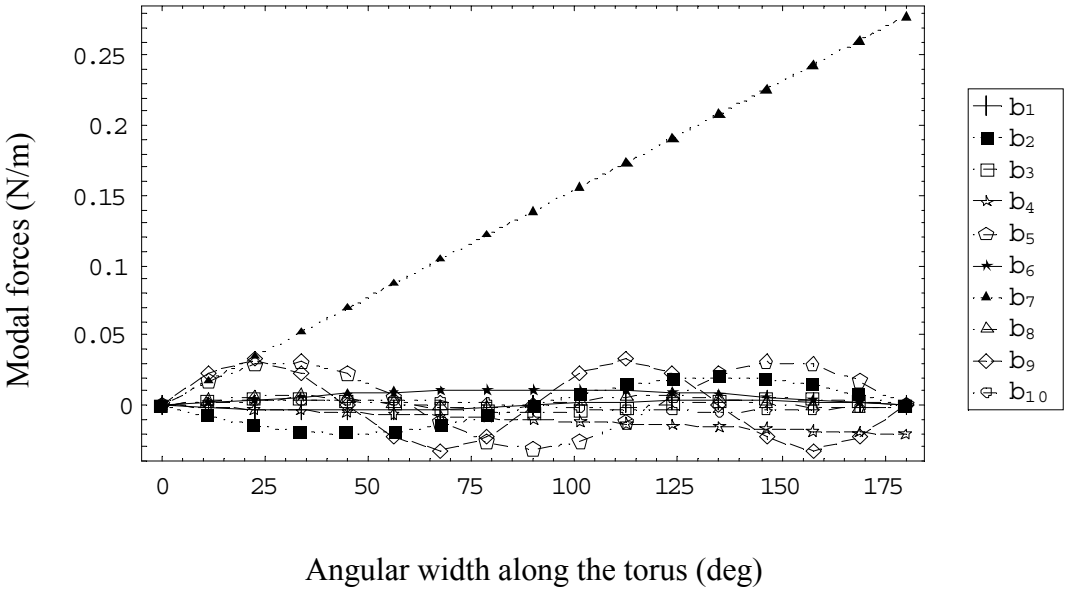

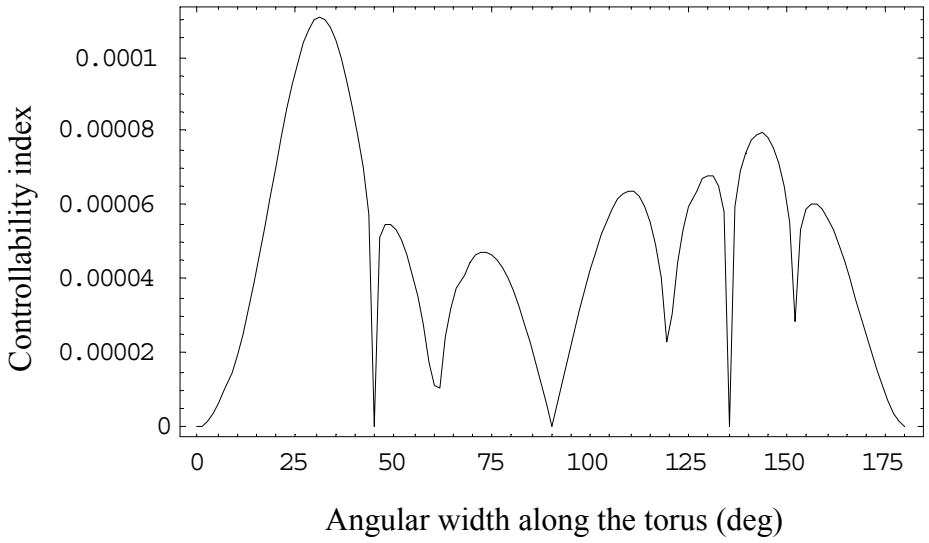

Fig. 5.6: Modal forces at unit voltage and controllability index for an actuator as the angular width q_2 varies from 0 to 180^o along the torus.

Now we study the effects of locations and size of the piezoelectric sensors. Due to the very small thickness of the patch and the shell, the effects of bending strains on the sensor voltage are found to be negligible. In addition, from the expressions of the strains, we find that symmetric and antisymmetric modes will produce symmetric and antisymmetric strains, respectively. This implies that the behavior of a modal sensor voltage will be similar to that of the corresponding mode. This also indicates that most of the explanation given for the actuator will hold for the sensor too. Figure 5.7 shows the modal sensing constant as the sensor location is changed along the ϕ-direction. Modal sensing constants 2, 5, 7, and 9 demonstrate symmetric behaviors and the others behave antisymmetrically. Similar to the controllability index, the observability index is also symmetric about $\phi = 0^o$ and 180^o and shows peaks. As described earlier, a high observability index corresponds to those locations where all the modes can be sensed properly. At $\phi = 0^o$ and 180^o, sensor voltages due to antisymmetric modes are zero. This leads to zero observability index at these locations. The peak values are only at those locations where all the modal sensor voltages are nonzero. Figures 5.8 display the sensor behavior as its angular width is changed from 0^o to 360^o. Figures 5.9 and 5.10 show how the size and location along the *s*-direction affect the sensor constants and observability index. Similar to the actuator behavior, we see that a patch of larger length and width might not always yield better sensing capabilities and the modal sensing constants are very sensitive to the location and size. For a toroidal shell, the Lamé parameter A_ϕ is a constant (Eqs. 4.1). Hence all the terms corresponding to the displacement u_s in the expressions of the normal strains ε_ϕ and ε_s contain derivatives with respect to *s*. As mentioned earlier, in a purely torsional mode, the displacements u_ϕ and *w* are zero and u_s is independent of *s*. Thus, the normal strains for a purely torsional mode will be zero. Due to this, a piezoelectric sensor with a hexagonal symmetric structure cannot detect a purely torsional mode. However, this will not cause a problem as this type of mode occurs at relatively high frequencies (above 100 Hz for the present case). Similar situations occur in the case of an axisymmetric torsional mode of a circular cylinder (Callahan and Baruh, 1999) and in-plane torsional vibration of a plate (Lee, 1990). One can also see that this type of sensor cannot detect the rigid-body modes either as these modes do not produce any strains.

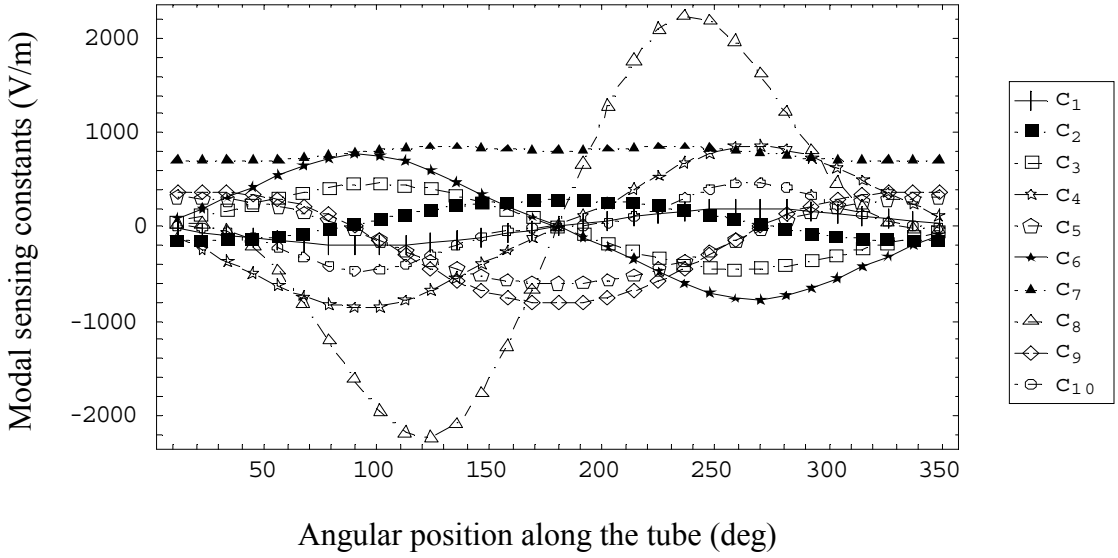

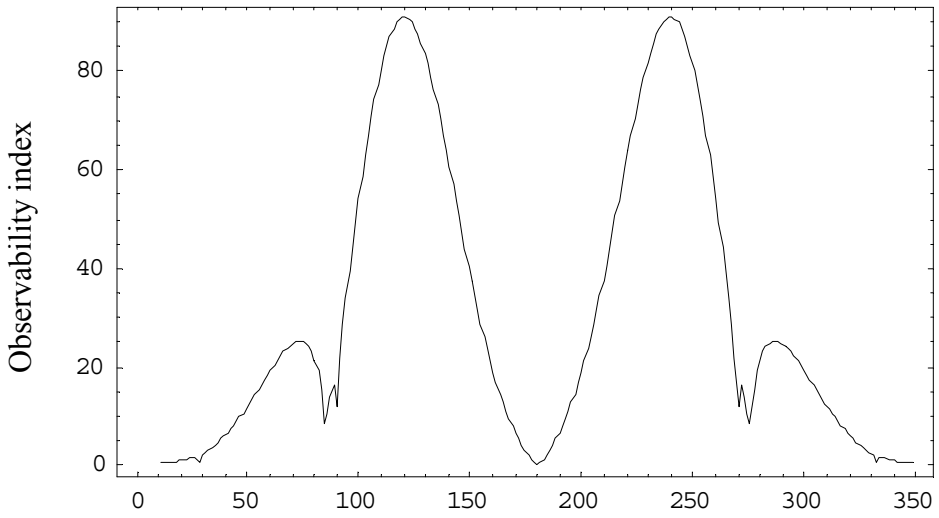

Fig. 5.7: Modal sensing constants and observability index for a sensor as its location is changed from $\phi = 0$ to 360^o along the tube of the torus.

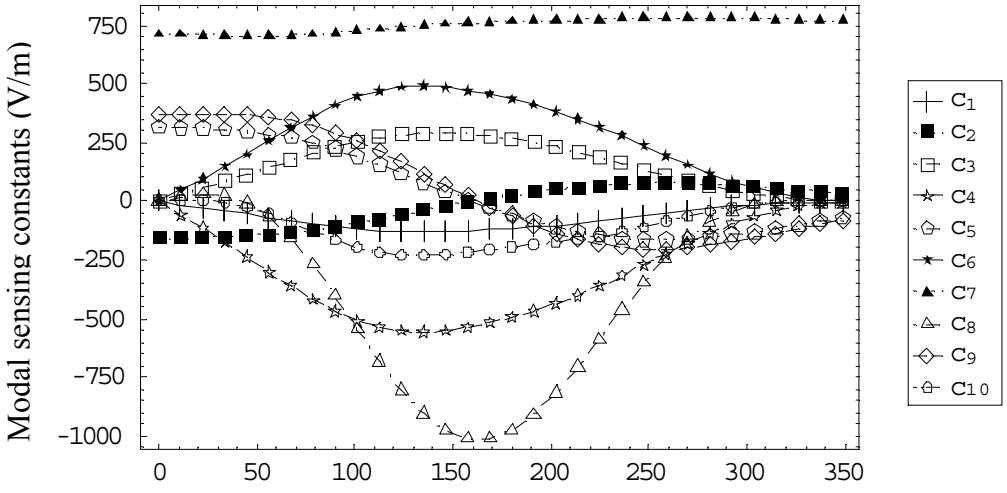

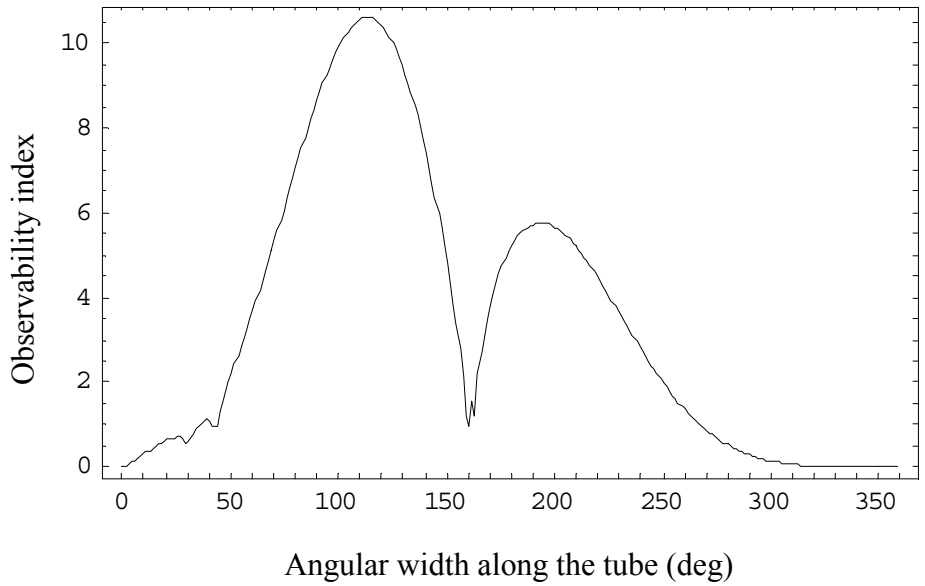

Fig. 5.8: Modal sensing constants and observability index for a sensor as its angular width f_2 varies from 0 to 360^o along the tube of the torus.

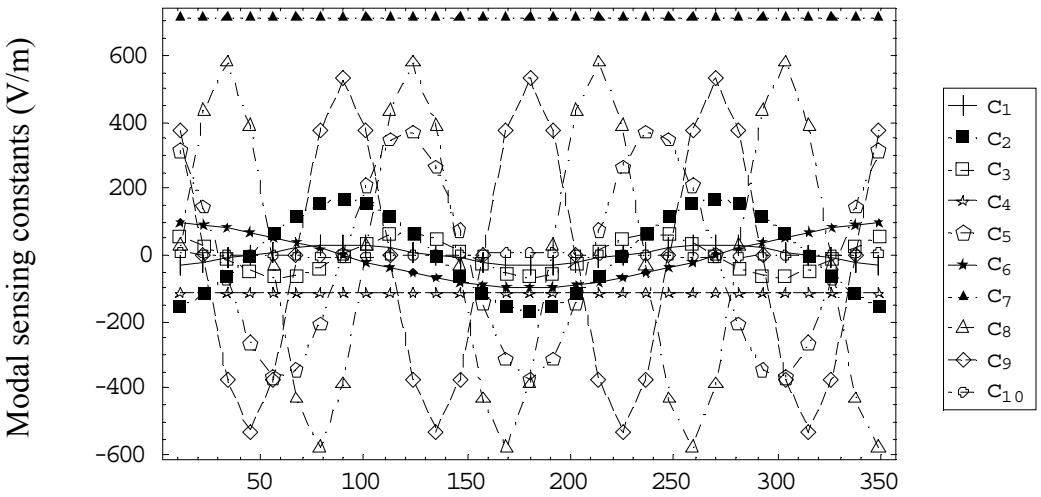

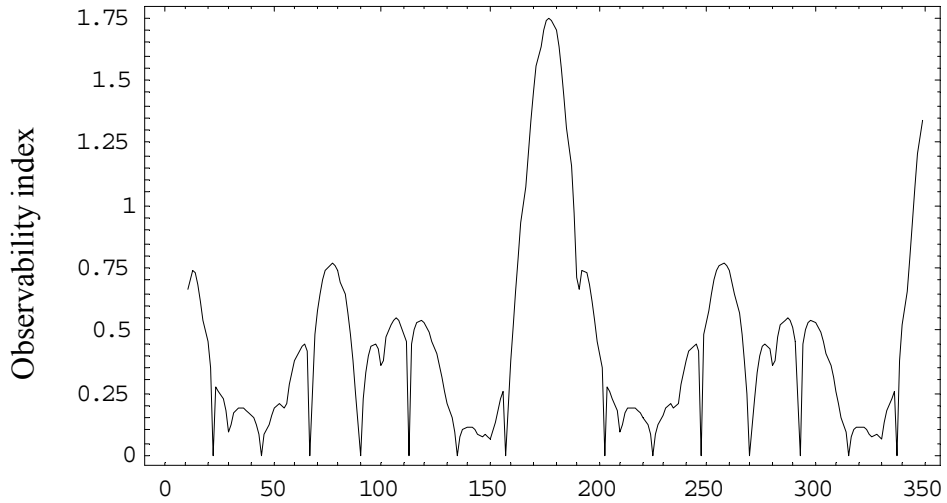

Fig. 5.9: Modal sensing constants and observability index for a sensor index as the location of a sensor is changed from $q = 0$ to 360^o along the torus.

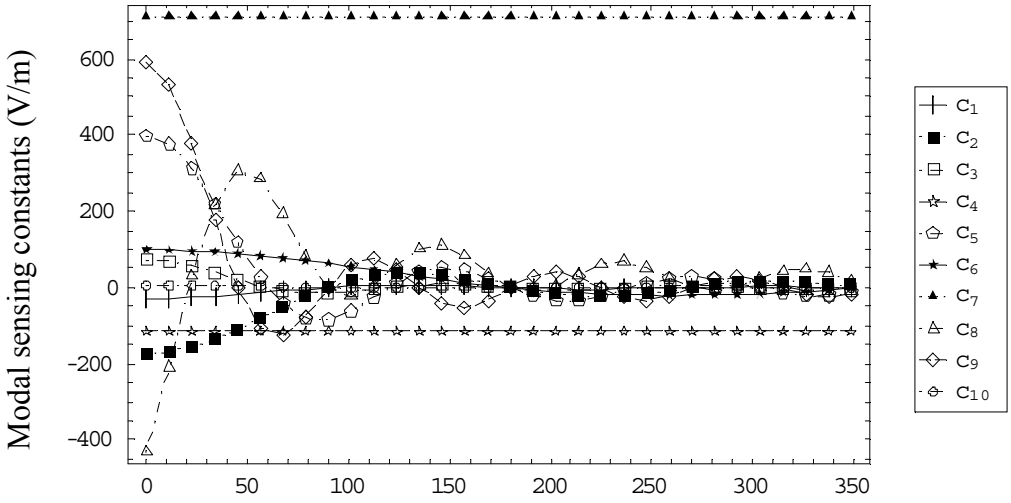

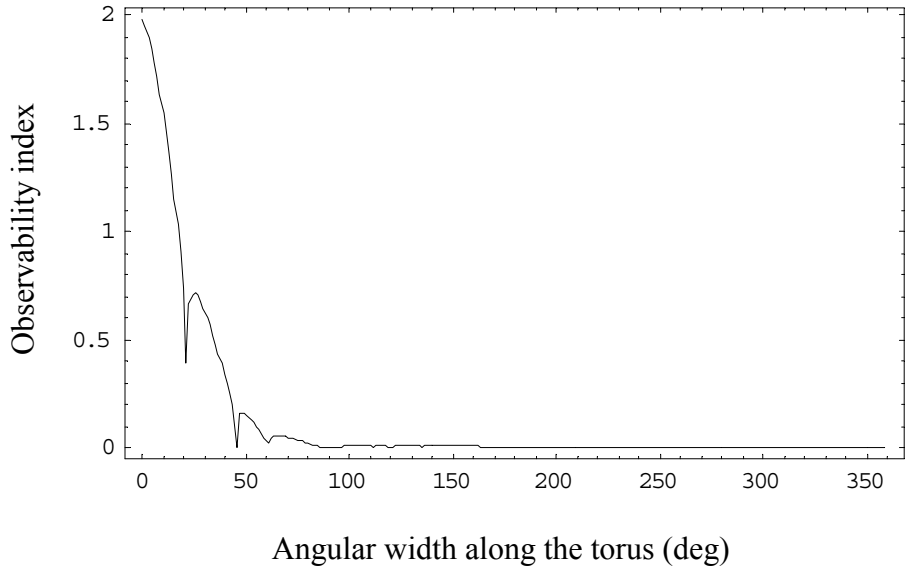

Fig. 5.10: Modal sensing constants and observability index for a sensor as its angular width q_2 varies from 0 to 360^o along the torus.

5.5 Genetic Algorithm

In Chapter 4, we explained that most of the natural frequencies of the torus are repeated once and several of them are close. This implies that one will need multiple actuators and sensors. From the discussion in the above section, one can conclude that the performances of actuators and sensors are quite complicated. This makes the selection procedure of the actuators and sensors difficult and necessitates the use of some kind of optimization procedure. We will use a genetic algorithm (GA) for selecting optimal actuators and sensors. The most attractive feature of a GA is that it does not need derivatives or any auxiliary information about the objective function to be optimized. This makes its application for even a complicated problem, e.g., a nonlinear and discontinuous objective function, comparatively easy. Another characteristic of a GA is that the search direction for the optimal solution is random and not the same for all points of the solution space. Here, we present a brief overview of a GA.

A genetic algorithm is a heuristic procedure for global search and optimization in a multi-parameter search space, based on the mechanics of natural genetics. It starts with a population of randomly generated solutions and advances towards better solutions by applying the so-called genetic operators (reproduction, crossover, and mutation), mimicking a natural genetic selection and evolution process (Goldberg, 1989). After the applications of these operators, the elements (chromosomes) of the population, as a whole, acquire better properties and more suitability and come to the next stage, called generation. In each generation, the good solutions pass on to the next generation with a higher probability than the bad solutions. A fitness function is used in evaluating the quality of a chromosome and then the operators perform the tasks of exchanging the information among the chromosomes, randomly changing some of their properties, and copying the chromosome for the next generation. Usually, the number of chromosomes in the subsequent generations is kept constant. The population undergoes several generations till the solutions converge or the maximum number of iterations has been reached. The best solution of these generations is chosen as the final solution.

The variables of the optimization problem can be either represented by real numbers, called real-coded GA, or by strings of binary numbers, called binary-code GA. In this work, we use binary-coded GA, where different sections of a string contain information about different variables. Each section is comprised of several binary bits (0 or 1). The number of binary bits in a section depends upon the desired accuracy in the final solution. In this study, the piezoelectric patches are assumed to be of the shapes of generalized rectangles in the curvilinear coordinate systems of the shell. Hence, each patch can be specified by four numbers (ϕ_1^m, ϕ_2^m, s_1^m, and s_2^m). We also take all the actuators to be of the same size and all the sensors to be of the same size. The size of a patch can be determined using the angular widths in the ϕ- and s- directions. Once the size is determined, we need only two variables to specify the spatial distribution of a patch. Hence for n patches we have $2n+2$ variables to determine. Each variable is represented by *10* bits. The value of a variable can be determined by decoding the binary string of the corresponding section of the chromosome. The goal is to maximize the controllability (observability) index of actuators (sensors). The formulation of the controllability (observability) index serves as the objective function. The objective values of the chromosomes are normalized between *0* and *1* using a linear scale, keeping the proportion of each datum to the mean constant. The resulting number is termed as the fitness value of the actuators/sensors. The fitness values of chromosomes are then used in the three genetic operators.

The first genetic operation done on the array of fitness values is what is known as reproduction. It involves selection of chromosomes and copying them to a matting pool. It chooses a new population from an old population, with the frequency of reproduction of chromosomes proportional to their fitness values. First, a "running sum" of the fitness values in the population is calculated; for example, four chromosomes with the fitness values *0.4*, *0.2*, *0*, and *0.9* will give the running sum as *0.4*, *0.6*, *0.6*, and *1.5*. Random numbers up to the total fitness are generated and indexed into the running sum. The corresponding chromosome from the input population is then selected. Thus, the prospect of getting a copy of a particular chromosome in the matting pool depends upon how high the fitness value of that chromosome is. This idea is essentially based on the survival-of-the-fittest philosophy in natural selection.

The next genetic operation performed is the so-called crossover. It provides a mechanism for the strings to mix their qualities through a random process. Unlike the reproduction operation, which just copies the old chromosomes in the new generation, the crossover operation creates new chromosomes. Two strings are picked from the matting pool at random and some portions of the strings are exchanged between the two strings. The effect of crossover may be good or bad. Thus, in order to preserve some of the good strings of the previous generation, not all strings in the matting pool undergo crossover. The number of crossover operations is dependent upon the crossover probability (p_c). Approximately, $100 \times p_c$ % of the strings are used in the crossover and the rest remain unchanged (Deb, 1996).

The last operation performed on the strings is mutation. It enhances the ability of the GA to find the near-optimal solutions. Mutation is an occasional alteration of the value of a bit at a randomly chosen position of a string and usually take place with a small probability (p_m). It creates a solution in the neighborhood of the current solution, thereby achieving a local search around the current solution. This also helps maintain diversity in the population.

5.6 Optimal Size and Placement

5.6.1 One Actuator and One Sensor

The application of the GA is first demonstrated using one actuator and one sensor with the first ten modes of vibration. This part of the work is mostly concerned with qualitative analysis and hence, for simplicity, we consider only one from every pair of repeated modes. Moreover, the passive effects of the actuators/sensors will not be considered. Table 5.3 shows the values of parameters used in the GA.

Figure 5.11 illustrates the selection of the actuator. The average and the best controllability index of the population are plotted against the number of iterations in Fig.

5.11-a. It can be seen that as the population goes through the subsequent evolution process, the best controllability index of the population increases for up to 50 iterations and then remains almost constant. This indicates that the genetic operators successfully increase the quality of the solution as the population goes through the different iterations, and ultimately the solution converges. The average controllability index also follows a similar pattern but it is oscillating after 50 iterations. This is because the population has attained the near maximum value of the controllability index in the first 50 iterations and any subsequent changes due to the different operator make the population as a whole fluctuate near its optimum value. Figure 5.11-b shows the final location of the actuator corresponding to the best chromosome of the population history. It also shows the actuator corresponding to the best location of the first generation, i.e., the initial population. Controllability indices for the two actuators are plotted in Fig. 5.11-c in order to demonstrate the use of the optimization technique. While the first bar in every group of the modal forces represents the modal forces due to the initial actuator, the second bar is due to the optimal actuator. Clearly, there is improvement in the modal forces. A similar phenomenon can be noted in the selection of a sensor (Fig. 5.12). It can be seen that the modal sensing constants are higher for the optimal sensor than the initially chosen sensor. The important difference between the optimal actuator and optimal sensor is that while the former tends to attain a larger size, the latter acquires a smaller size.

Table 5.3: Values of different parameters used in GA for one actuator and one sensor.

Parameter	**Values**
Population size	15
Maximum number of iterations	200
Maximum circumferential width of the patch	$\pi R/4$
Maximum meridional width of the patch	$\pi/4$
Crossover probability (p_c)	0.5
Mutation probability (p_m)	0.005

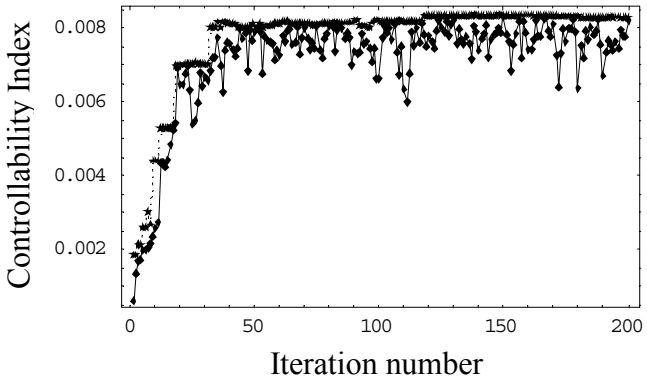

(a) Mean value (lower curve) and the best value (upper curve) of the population vs. iterations

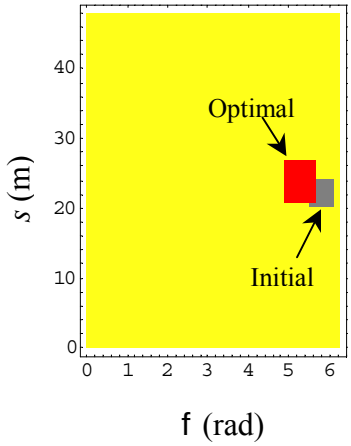

(b) Initial (lower) and the optimal (upper) locations and sizes of an actuator.

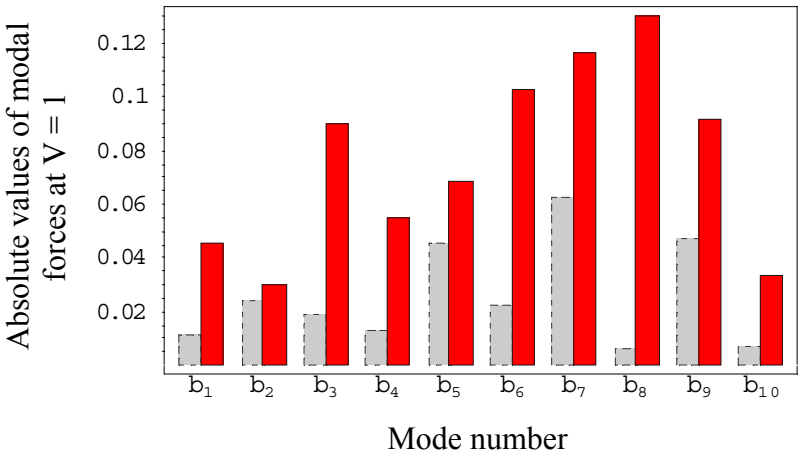

(c) Modal controllability corresponding to an actuator selected initially (first bar) and optimally (second bar).

Fig. 5.11: Optimal size and placement of an actuator considering the first ten modes with no repeated frequencies.

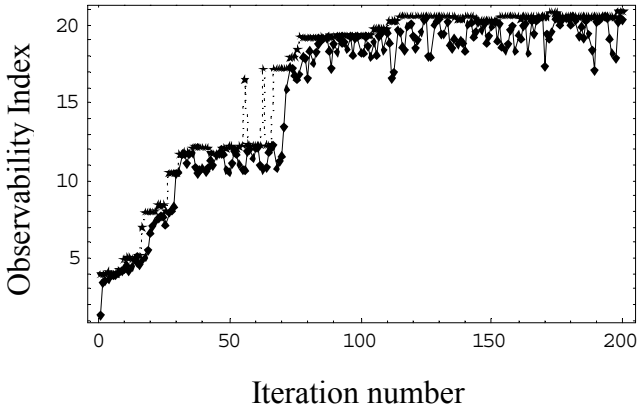

(a) Mean value (lower curve) and the best value (upper curve) of the population vs. iterations

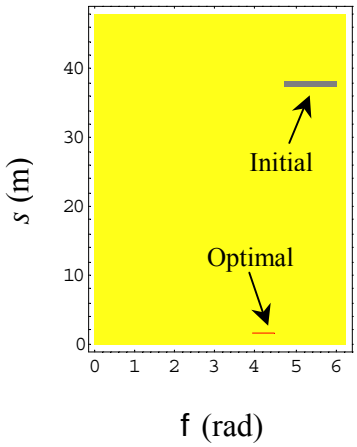

(b) Initial (lower) and the optimal (upper) locations and sizes of a sensor.

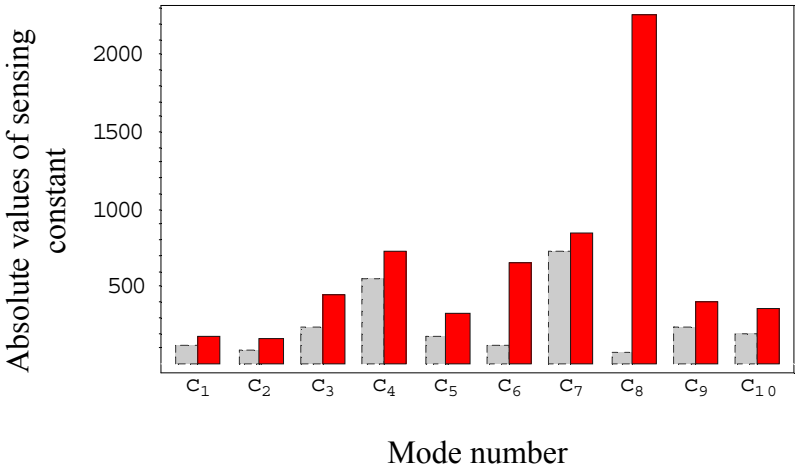

(c) Modal observability corresponding to a sensor selected initially (first bar) and optimally (second bar).

Fig. 5.12: Optimal size and placement of a sensor considering the first ten modes with no repeated frequencies.

5.6.2 Five Actuators and Five Sensors

The analysis in this section will be used in the final control problem. We consider the first nine modes in this study, which will be all the modes (including the orthogonal pairs of modes) below *20* Hz. From Fig. 4.5, we can see that the first nine modes will consist of four symmetric modes and five antisymmetric modes. Out of these nine modes, one will be axisymmetric and the rest will be non-axisymmetric. Also from Fig. 4.5, taking into account the repeated modes, we see that there are two antisymmetric modes at 17.71 Hz, one axisymmetric mode at 17.85 Hz, and two symmetric modes at 18.55 Hz. This means that there are five modes within a range of 0.84 Hz. From linear control theory, we know that to control the modes with the repeated frequencies, one needs to consider multiple actuators and sensors. The numbers of the actuators/sensors must be at least the same as the multiplicity of the frequencies. These five frequencies, though not exactly repeated, can be considered close enough to necessitate five actuators and five sensors. Going by the minimum number of actuators and sensors required, we will try to find optimal locations and sizes of five actuators and five sensors in this study.

Table 5.5 shows the parameters of the GA used in finding the optimal actuators and sensors. It can be seen in the table that the maximum circumferential and meridional widths have been chosen to be small. This is done so as to have minimal passive effects of the actuators. The population time history is plotted in Fig. 5.13-a and the optimum actuators are shown in Fig. 5.13-b. Similarly, Fig. 5.14 shows the five optimal sensors and the search history. Note that in the vibration control problem, discussed in the next chapter, we will consider these nine modes along with the optimal actuators/sensors found in this section.

Table 5.4: Values of different parameters used in GA for five actuators and five sensors.

Parameter	Values
Population size	30
Maximum number of iterations	600
Maximum circumferential width of the patch	$\pi R/16$
Maximum meridional width of the patch	$\pi/8$
Crossover probability (p_c)	0.5
Mutation probability (p_m)	0.005

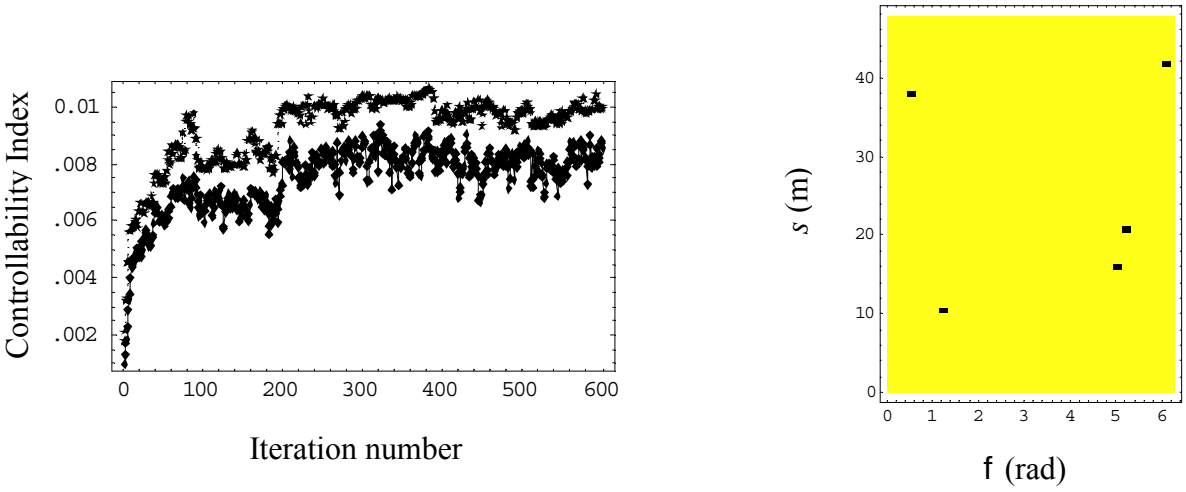

(a) Mean value (lower curve) and the best value (upper curve) of the population vs. iterations

(b) Optimal locations and sizes of the five actuators

Fig. 5.13: Finding five optimal actuators using a GA

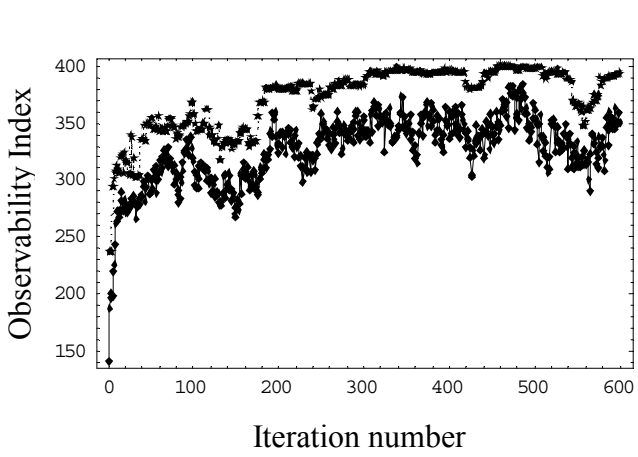

(a) Mean value (lower curve) and the best value (upper curve) of the population vs. iterations

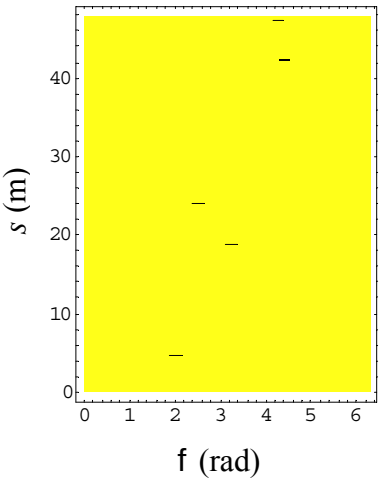

(b) Optimal locations and sizes of the five sensors

Fig. 5.14: Finding five optimal sensors using a GA

5.7 Passive effects of the Actuators and Sensors

Before we use the above analysis, we investigate the passive effects of the actuators and sensors. Comparing the data in Table 4.4, which shows the physical properties of the inflated torus, and Table 5.1, which shows the physical properties of MFC^{TM} actuators, we see that the actuators have much higher density and elastic modulus than the inflated torus. This means that these actuators are likely to change the physical properties of the bare inflated torus. To quantify these changes, we calculate the natural frequencies and mode shapes of the inflated torus with the attached actuators. It should be recalled here that for a bare toroidal shell for which the material properties are the same everywhere, the displacement fields in the s-direction can be given by sinusoidal functions and the displacement fields in the ϕ-direction can be separated into two groups, called symmetric and antisymmetric modes (Chapter 4). Once the patches are attached, the displacement fields lose these properties. Therefore, for a more accurate analysis, one will have to express the displacement fields in terms of double Fourier series, i.e., Fourier series in both ϕ- and s -

directions. This makes the free vibration analysis computationally very expensive. We ignore these changes and use the same approach as suggested in Chapter 4. It should be noted from Table 5.5 that there is an appreciable change in the natural frequencies. It should be noted that the due to the high density of the MFC^{TM} actuators, they behave like concentrated mass. The MFC^{TM} actuators also change the stiffness of the structure. From Table 5.5, it can be observed that the mode shapes also change due to MFC^{TM} actuators. In the control problem, we will use the changed natural frequencies and the mode shapes of the torus. It should be noted that the elastic modulus and density of the PVDF material is of the same order as that of the inflated torus. However, due to small sizes, the passive effects of the sensors are found to be negligible. Therefore, passive effects of the sensors will not be considered.

Table 5.5: Comparison of natural frequencies with and without the passive effects.

Mode Number	Wave number, symmetry	Frequencies without the passive effects (Hz)	Frequencies with the passive effects (Hz)
1	2, Antisymmetric	6.90	8.24
2	2, Antisymmetric	6.90	8.24
3	2, Symmetric	7.24	6.06
4	2, Symmetric	7.24	6.06
5	3, Antisymmetric	17.71	14.73
6	3, Antisymmetric	17.71	14.73
7	0, Antisymmetric	17.85	18.45
8	3, Symmetric	18.55	14.42
9	3, Symmetric	18.55	14.42

5.8 Conclusions

In this chapter, we found optimal sizes and locations of actuators and sensors. First, we computed modal forces and modal sensing constants for one actuator and one sensor. In order to evaluate the performance of the actuators/sensor considering several modes, we presented the definitions of controllability and observability indices. We found that, due to the small thickness of the patch and the shell, a bimorph configuration does not provide any better actuation than a unimorph. Thereafter, we obtained the modal forces, modal sensing constants, and the performance indices for an actuator and a sensor of different sizes and placed at different locations. It was seen that modal forces and modal sensing constants have the same type of symmetry around the tube as the mode to which they belong. Performance indices show the advantageous positions of the actuator and sensor. Another important result from this analysis is that a higher patch area may not provide better actuating and sensing capabilities. Finally, we showed that the sensor structure considered in this study could not detect purely torsional and rigid body modes. Thereafter, we outline the basics of a GA and obtain an optimal actuator/sensor for the first ten modes without considering the repeated modes due to the axisymmetric nature of the torus. It was shown that the optimal actuator/sensor gives higher performance indices. Next, the optimization method was applied to find five actuators and five sensors considering the first nine modes including the repeated modes. The actuator sizes were kept small so that its passive effects are small because of high elastic modulus and density of the MFC^{TM} actuators. It was shown that the mass and stiffness effects of the actuators are important. However, the passive effects of the sensors, made of PVDF material, are found to be negligible. The five optimal actuators and sensors along with the modified natural frequencies and mode shapes due to the passive effects of actuators will be used in the vibration control problem, described in the next chapter.